Thermodynamics of Unstable DNA Structures from the Kinetics of the Microgene PCR

Mark Itsko,*,§,† Arieh Zaritsky,† and Avinoam Rabinovitch‡

Departments of Life Sciences and Physics, Ben-Gurion University of the Negev, P.O. Box 653, Be'er-Sheva 84105, Israel

Received: May 21, 2008; Revised Manuscript Received: July 24, 2008

The microgene polymerization reaction (MPR) generates head-to-tail tandem repeats from homoduplexes (HDs). In MPR initiation, one HD putatively aligns two others in the proximity required to form a nucleation complex, thus allowing the DNA polymerase to skip the intertemplate gap and generate an initial doublet (ID) prone to repeat propagation. The current investigation refines this stage by additional thermodynamic considerations and elucidates the fundamental mechanism underlying propagation. Four different HD types were designed to extend the range of melting temperatures and to simultaneously modify the stabilities of their secondary structures. Following the propagation kinetics with these, using real-time PCR at different temperatures revealed a new stage in the MPR, amplification of an ID by an original HD, and enabled us to decipher the biphasic kinetics of the process. This amplification merges with the propagation stage if the lifetime of the staggered conformation of the ID is sufficiently long for DNA polymerase to fill in the overhangs. The observed increase with temperature of thermodynamically unfavorable conformations of singlet and doublet HDs that underlies, respectively, MPR initiation and propagation is well correlated with simulations by UNAFold.

Introduction

The microgene polymerization reaction (MPR) generates multiple head-to-tail tandem repeats in PCR from a pair of fully- or partially- complementary oligonucleotides. This phenomenon was originally described by Shiba et al.[1] and is utilized to produce artificial proteins containing repetitive motifs with useful properties[2−4] or to expose cryptic activities of inactive proteins.[5] Successful exploitation of the MPR for protein engineering or other purposes requires deep understanding of the underlying processes. Expansion of different oligonucleotide repeats in human genome is known to cause inherent diseases.[6−8] The expansion propensity of different tetra-nucleotides is sequence-dependent but the source of this dependence is still enigmatic.[9]

Repeat propagation in MPR obviously involves slippage of the complementary strands, thus generating overhangs that are filled in by DNA polymerase. Such a mechanism was proposed for repeat expansion both in vivo, for example, in human genome,[10] and in vitro, in repeats-containing homoduplexes (HDs).[11] However, the expansion of nonrepetitive HDs into multiple repeats is not so obvious. It has been proposed that they must first be duplicated in a head-to-tail manner (Figure 1, top panel) to generate a minimum repetitive unit prone to expand.[1] Generation of an initial doublet (ID) out of a HD (initiation of the MPR) is thus a crucial stage, the mechanism of which is intriguing since it ostensibly implies existence of "illegitimate blunt-end ligating activity" of DNA polymerase that allows it to skip the gap between two discontinuous templates.

Kinetic analyses of the total MPR products amplified by real-time PCR at varying HD concentrations have disclosed a molecularity of about 3.1 for the initiation in nonrepetitive HDs,[12] meaning that 3 HD molecules are engaged in ID formation. A simple model for this engagement that forms a so-called nucleation complex (NC) depicts one HD (original singlet OS) aligning and bridging the other two, fixing them in a proximity required for the DNA polymerase to skip the intertemplate gap (Figure 1, top panel). The bridging may occur through a set of occasional Watson−Crick bonds of very low stability, that is, with an absolute value of ΔG at least 1 order of magnitude lower than that of the fully paired primer (OS). This head-to-tail tandem repeat-generation, although rare, is exponentially amplified and can therefore be detected experimentally and evaluated analytically.

The simple approach to test this model is by comparing efficiencies of the MPR with OS sequences having different tendencies to form NC. Modifying the sequence to eliminate certain secondary structures generates others with different melting temperatures T_m, which also affect the MPR efficiency.[12] Another approach to test and refine the model is proposed here, to follow, at varying temperatures, the existence of the putative NC of different OS types with RT-PCR.

Experimental Methods

End-Point Detection PCR. A 50 μL reaction mixture contained 560 pmol of the OS-forming strands (Table 1), dNTP (500 μM each), ThermoPol buffer, 6 mM $MgSO_4$, and 2 units of Vent polymerase. The conditions for T-Gradient Thermoblock cycler (Biotron, Germany) were 10 min at 95 °C, then 65 cycles of 20 s at 95 °C, and 1 min at a temperature near T_m for 10 μM of each OS, that is, 68 °C (for NOMUL), 69.2 °C (NOMU), 72 °C (EVNA) and 74 °C (EVNAH). The amplicons were heated to 95 °C for 10 min, rapidly cooled in icy water,[13] resolved with EtBr-stained 2.5% agarose gel, UV-illuminated, and digitized. The intensity values of the bands, obtained by ImageJ

* To whom correspondence should be addressed. Tel: 972-8-6461 712. Fax: 972-8-6278 951. E-mail: ariehz@bgu.ac.il.
† Department of Life Sciences.
‡ Department of Physics.
§ Current Address: Laboratory of Molecular Genetics, National Institute of Environmental Health Sciences, Research Triangle Park, NC 27709.

10.1021/jp8045142 CCC: $40.75
Published on Web 09/17/2008

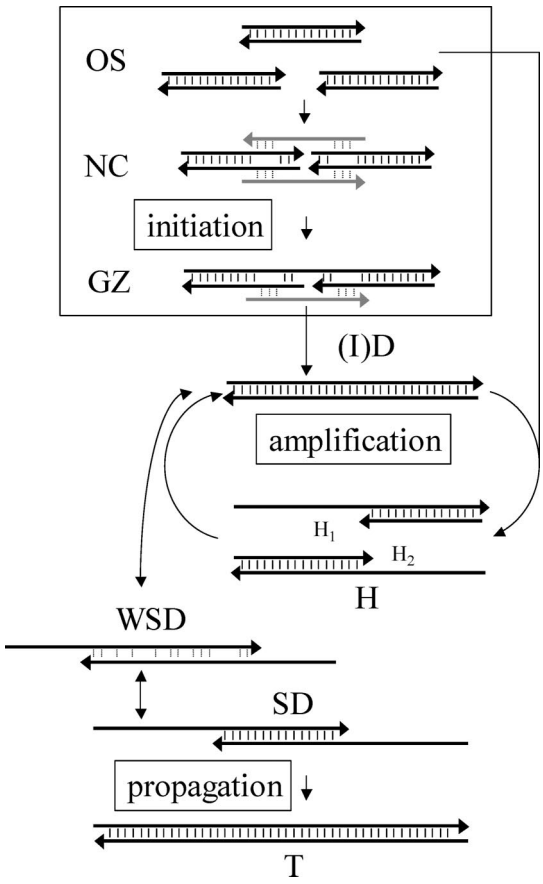

Figure 1. A model for the MPR with nonrepetitive HDs. Initiation: OS, original singlet HDs (a pair of complementary primers); NC, nucleation complex (an arrangement of three OS); grey strands correspond to the OS bridging the gap; GZ, gap zipper (conformation composed of half NC (hNC) and a DNA polymerase-generated (by gap skipping) single strand of ID). Amplification: (I)D, (initial) doublet; H_1 and H_2, hybridized denatured D and OS. Propagation: SD, staggered re-annealed D; WSD, weak SD (an unstable intermediate between D and SD); T, triplet. Arrowheads denote 3′.

(http://rsb.info.nih.gov/ij/), were normalized to OS in the respective untreated samples.

Real-Time (RT) PCR. The MPR total product was quantified in the ABI Prism 7000 sequence detection system (Applied Biosystems) using Absolute QPCR SYBR Green ROX Mix (ABgene, Surrey, U.K.). Hexaplicates, consisting of 10 μL of "Absolute Mix" and 10 μL of the respective OS (3.2 pmol), were thermally cycled 15 min at 95 °C, 65 rounds of 15 s at 95 °C, and 3 min at the indicated temperature. The T_m of each OS at 160 nM (= 3.2 pmol 20 μL^{-1}) was determined by the dissociation protocol of the cycler. The OS double-stranded fraction was estimated by the relative area under the melting profile, approximated by the normal curve, cut off at any given temperature (Figure 5A). The threshold cycle *N*th was arbitrarily determined at a net fluorescence value of 0.2 because the initial SYBR Green fluorescence exceeds that of ROX. The exponential range in the MPR expansion curves was used to evaluate the process amplification rate A [$= \ln(1 + E)$], where E is the amplification efficiency (Appendix).

Simulations in Silico. UNAFold 3.4 (http://dinamelt.bioinfo.rpi.edu/download.php) and Visual OMP6 (http://www.dnasoftware.com/) were used to predict second-rank conformations of OS (D) and calculate the ΔG of their formation, respectively, at different temperatures in 160 nM HD, 50 mM Na^+, and 8 mM Mg^{2+}.

Results

MPR Kinetics and Its Characteristics. Generation of MPR products from each OS (Table 1) displayed biphasic kinetics (e.g., gray arrow in Figure 2A) with NOMUL, EVNA, and EVNAH at temperatures just above their corresponding T_m, whereas single-burst kinetics (e.g., black arrow) was observed at temperatures far above T_m for these three OS types and at all temperatures for NOMU (Figure 2A).

The amplification efficiency (E; fraction of product added per unit time, derived from the process amplification rate A [$= \ln(1 + E)$]; see Appendix) and threshold cycle (*N*th; cycle number at which the signal is first detected) depend on the proximity of the experimental temperature to T_m. Comparing the dependencies is enhanced by transforming the scale from temperature to fraction of double-stranded OS at each temperature (Figure 2B). With all four types, at about 10% (see also Figure 5A), E and *N*th reach minima and maxima, respectively. It was impossible, however, to analyze these characteristics at temperatures below T_m (fraction of above 50%) because then, the ever-growing fluorescence background leads to underestimated E and overestimated *N*th.

Amplification and Propagation of Doublets. The biphasic kinetics observed here (Figure 2A) is explained by two parallel processes (with distinct kinetic parameters) involved in the MPR expansion (Figure 1), amplification of the ID by the original primers (composing OS) through hybrids (H) and propagation of doublets (D) to triplets (T) and higher-level multiples through staggered conformations (SD). To demonstrate these thermodynamically unfavorable SD, the end products generated from all four OS types, with concentrations of the monomer substrates (nucleotides [dNTP]) that limit the extent of expansion[12] were heated at 95 °C and then quickly cooled in icy water. Of the four, the OS of NOMU was the only one to diminish (bottom band, lane 5 in Figure 3A), most likely due to its pairings with overhangs formed by staggered structures of multiple-repeated DNA. The treated samples of the other three OS displayed increased intensities of the D bands (84 bp, even number lanes in Figure 3A, compared with their counterparts), consistent with hybridization of tandem single strands of OS to a single strand of complementary D (e.g., the core of GZ in Figure 1) and with the explanation of the biphasic mode (Figure 2A).

To directly distinguish between the products of amplification and those of propagation, the experiment was stopped after 40 cycles, before the former process had supposedly been completed (Figure 3B). Under these circumstances, triplets (T) of NOMU are clearly produced earlier than in the other OS types. The disappearance of the biphasic kinetics (Figure 2A) at temperatures higher than 71 °C for NOMUL, 73 °C for EVNA, and 76 °C for EVNAH (Table 1) is thus explained by an increased probability of SD with temperature. The formation of SD is predicted by UNAFold to appear at a higher temperature than 73 °C for NOMUL, 78 °C for EVNA, and 80 °C for EVNAH (Figure 3C).

Estimation of the Ratio [ID]/[OS]. Estimating the ratio was based on backward extrapolation of the amplification curves to the first cycle.[12] The first burst in fluorescence intensity (Flu_{Tot}) observed (Figure 2A) was approximated by

$$Flu_{Tot} = Flu_{Bgr} \times (1 + (\gamma - 1) \times (e^{AN} - 1)/(R + e^{AN})) \quad (1)$$

(see Appendix), where Flu_{Bgr} is the intensity of the background fluorescence that corresponds to that of OS present in the system, γ is the ratio between the extinction coefficients of OS and D, R is the ratio between the initial [OS] and [ID], N is the PCR cycle, and A [$= \ln(1 + E)$] is the amplification rate. Least-

TABLE 1: The Original Singlets (OS) Used

Name	Sequence[a]	GC (%)	T_m (°C)[b]	ΔG_{OS}[c] (kcal mol^{-1})
NOMUL	5'-GGAAATAGAAGAACTTAAATCTTTATTAGAGATTAACACAGC-3' 3'-CCTTTATCTTCTTGAATTTAGAAATAATCTCTAATTGTGTCG-5'	28.6	67 (68)	-43
NOMU	5'-GGTGATAGAAGAACTTAAATCTTTATTAGGAATTAACCTGGC-3' 3'-CCACTATCTTCTTGAATTTAGAAATAATCCTTAATTGGACCG-5'	33.3	68 (68)	-45
EVNA	5'-GGTGATAGAAGTGCTTAAATCTTTATTAGGAATTGCTCTGGC-3' 3'-CCACTATCTTCACGAATTTAGAAATAATCCTTAACGAGACCG-5'	38.1	71 (72)	-48
EVNAH	5'-GGTGATAGTGCTGCTTTGATCTTTATTAGGAATTGCTCTGGC-3' 3'-CCACTATCACGACGAAACTAGAAATAATCCTTAACGAGACCG-5'	42.9	73 (74)	-50

[a] Bold-type letters indicate differences in composition between EVNA and NOMU. Underlined bold-type letters indicate differences in composition between NOMUL and NOMU and between EVNA and EVNAH. [b] Experimental and UNAFold-predicted (in brackets) melting temperature of the corresponding OS types. [c] Association free energy (Visual OMP6-predicted) of complementary strands into OS at 37 °C.

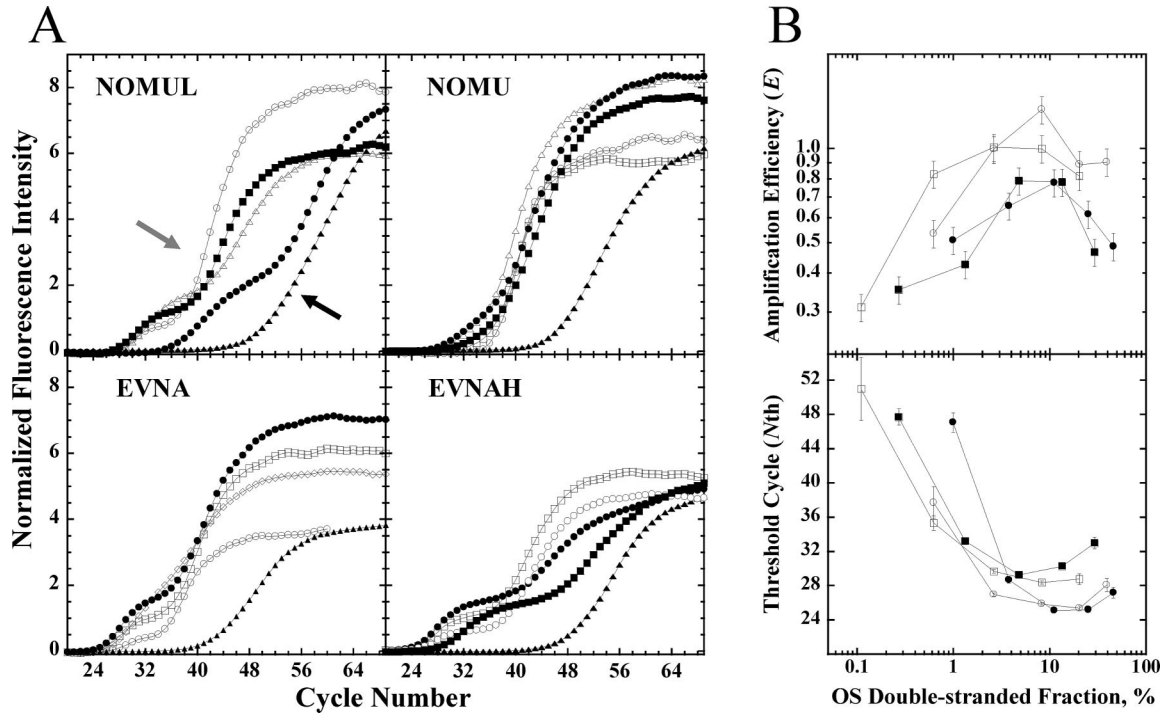

Figure 2. Kinetics of the MPR total product accumulation followed by RT-PCR at different temperatures (A) and the derived characteristics at varying extents of OS pairing (B). (A) MPR kinetics with four OS types, NOMUL (open circles, 68 °C; filled in squares, 69 °C; open triangles, 70 °C; filled in circles, 71 °C; filled in triangles, 72 °C), NOMU (open circles, 68 °C; open squares, 69 °C; open triangles, 70 °C; filled in circles, 71 °C; filled in squares, 72 °C; filled in triangles, 73 °C), EVNA (open circles, 71 °C; open squares, 72 °C; filled in circles, 73 °C; open diamonds, 74 °C; filled in triangles, 75 °C), and EVNAH (open circles, 71 °C; open squares, 72 °C; filled in circles, 73 °C; filled in squares, 74 °C; filled in triangles, 75 °C). Arrowheads point at biphasic (gray) and single-burst (black) kinetics. (B) *E* and *N*th, with the corresponding standard deviation shown as error bars, at different extents of temperature-dependent OS pairing: NOMUL, open squares; NOMU, closed squares; EVNA, open circles; EVNAH, closed circles.

square fits to the experimental results yielded values for γ, R, and A. Values of A in the Arrhenius plots for NOMUL and EVNAH (Figure 4A) were highly variable at each temperature, with correlation coefficients of around 0.9. The correlation coefficient for EVNA was even lower, and hence, its plot was not considered for analysis. The derived activation energy of amplification ($\Delta^{\ddagger}G_{ampl}$) is about -62 kcal mol^{-1}. The variability in changes of R with temperature (data not shown) is exceedingly high and not amenable for analysis, but its reciprocal R^{-1} is exponentially related to A for both OS types (Figure 4B). As A rose, the calculated ratios [ID]/[OS] declined, and over seven decades! Increased A corresponds to a decrease in the applied temperature (Figure 4A); hence, formation of ID is accelerated as temperature rises (Figure 4B). At each calculated A, the ratio [ID]/[OS] for NOMUL was lower than that for EVNAH. In addition, at $A = 0.46$ for NOMUL and 0.51 for EVNAH, the ratio lines were drastically bent.

Simulation in Silico of NC Formation at Different Temperatures. UNAFold predicts rather well the melting profiles for the descending parts of the curves using NOMU, EVNA, and EVNAH (Figure 5A) but underestimates the ascending parts of the corresponding curves, thus slightly overestimating T_m values (Table 1).

The most abundant structure predicted in the system at all temperatures is OS (closed squares in Figure 5B and C). As the temperature rises, different second-rank structures appear

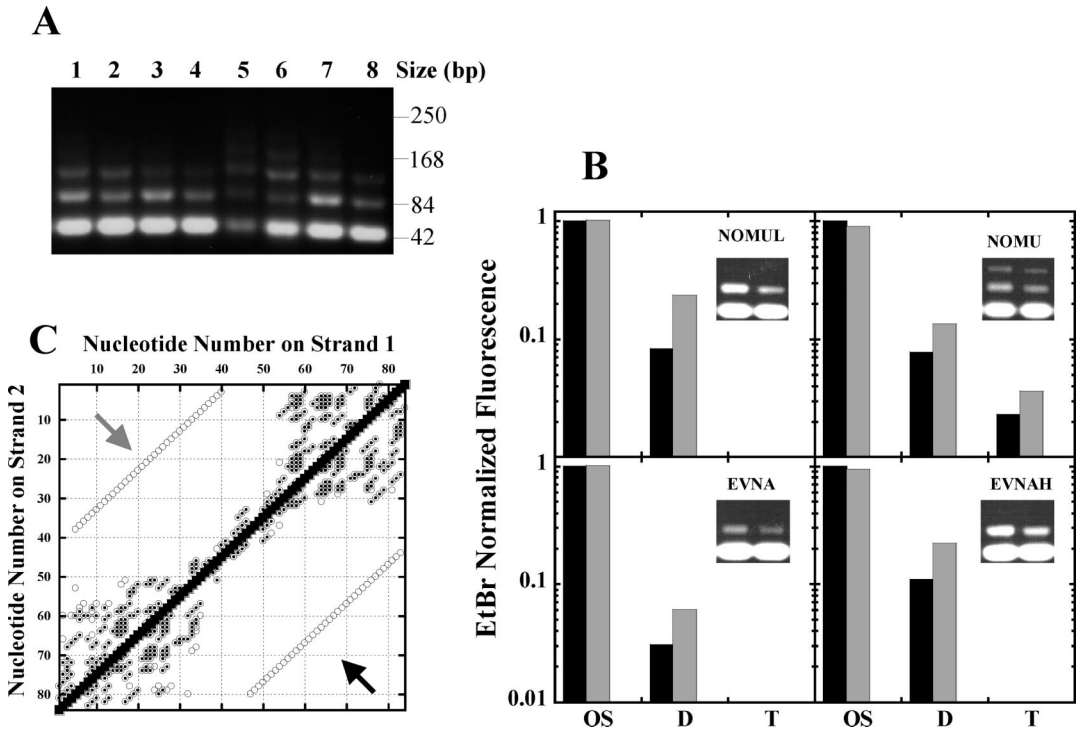

Figure 3. MPR-generated products after 65 (A) and 40 (B) PCR cycles from 4 OS types, separated on 2.5% agarose gel. (A) Lanes 1 and 2, with EVNAH; 3 and 4, EVNA; 5 and 6, NOMU; 7 and 8, NOMUL. Odd numbers designate samples denatured (10 min at 95 °C) and then cooled rapidly.[13] (B) Histograms of normalized integrated density (fluorescence of ethidium bromide, EtBr) of the bands (insets) corresponding to OS, D, and T with the denoted OS types, untreated (dark bar; right lane in inset) and treated (gray bar; left lane) as in (A). (C) Probability dot plot of hybridization (EVNAH's D). Each symbol designates pairing between strands' nucleotides. Filled in squares designate pairs existing in D at all tested temperatures with a probability close to 1. Open circles (enclosing dots or not, respectively) designate 2nd-rank pairs at 80 or 81 °C, with probabilities of approximately 10^{-6}. Arrows point at two lines corresponding to two SD, effective for propagation (black) and not (gray).

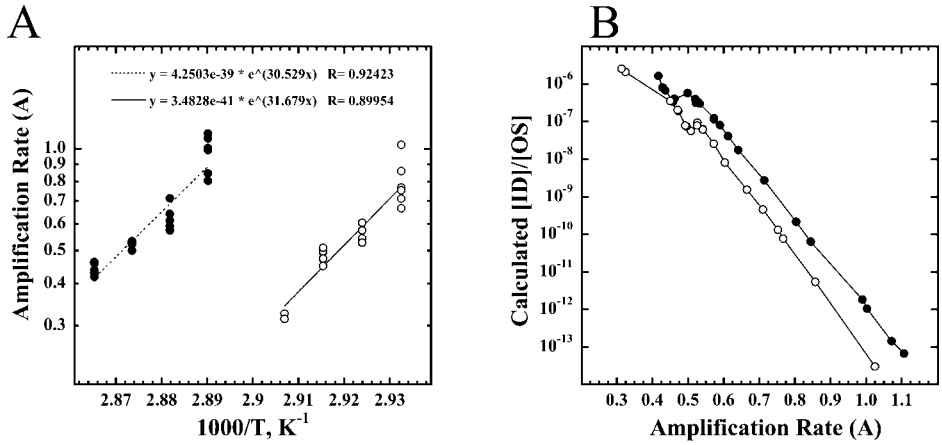

Figure 4. (A) Arrhenius plots of the MPR amplification rate, with NOMUL (open circles) and EVNAH (filled in circles). (B) Dependence of calculated [ID]/[OS] on the MPR amplification rate, with NOMUL (open circles) and EVNAH (filled in circles).

to compete. At the predicted T_m, 68 °C for NOMUL and 74 °C for EVNAH, many patterns of alternative pairings exist (dots enclosed in open circles), but none is effective for bridging leading to NC (Figure 1). The bridges appeared (dots enclosed in open squares and D in Figure 5) only above ~71 °C for NOMUL and 77 °C for EVNAH (3 °C higher than the corresponding predicted T_m values). The probability of NC-promoting structures rises as the temperature rises further (Figure 5E), which is consistent with the experimental observations (Figure 4B).

Discussion

Kinetics of the MPR. Existence of NC[12] as a necessary condition for ID formation in the MPR initiation (Figure 1) was challenged here by examining its probability at different temperatures. Since these ephemeral complexes are very scarce, their existence may be inferred by backward extrapolation of MPR kinetic curves. Simple extrapolation by an exponent was used to derive rough estimates of E at different temperatures, and the cycle number at a normalized fluorescence value of 0.2 was used as Nth. The derived E values are highly dependent on which points are chosen for fitting, and the artificial fluorescence level (0.2) for Nth detection can also be disputed. These values were therefore not used in the following analysis. However, their dependence on the OS double-stranded fraction is comparable (Figure 2B), thus justifying a similar approach to investigate the MPR with HD types having different T_m values.

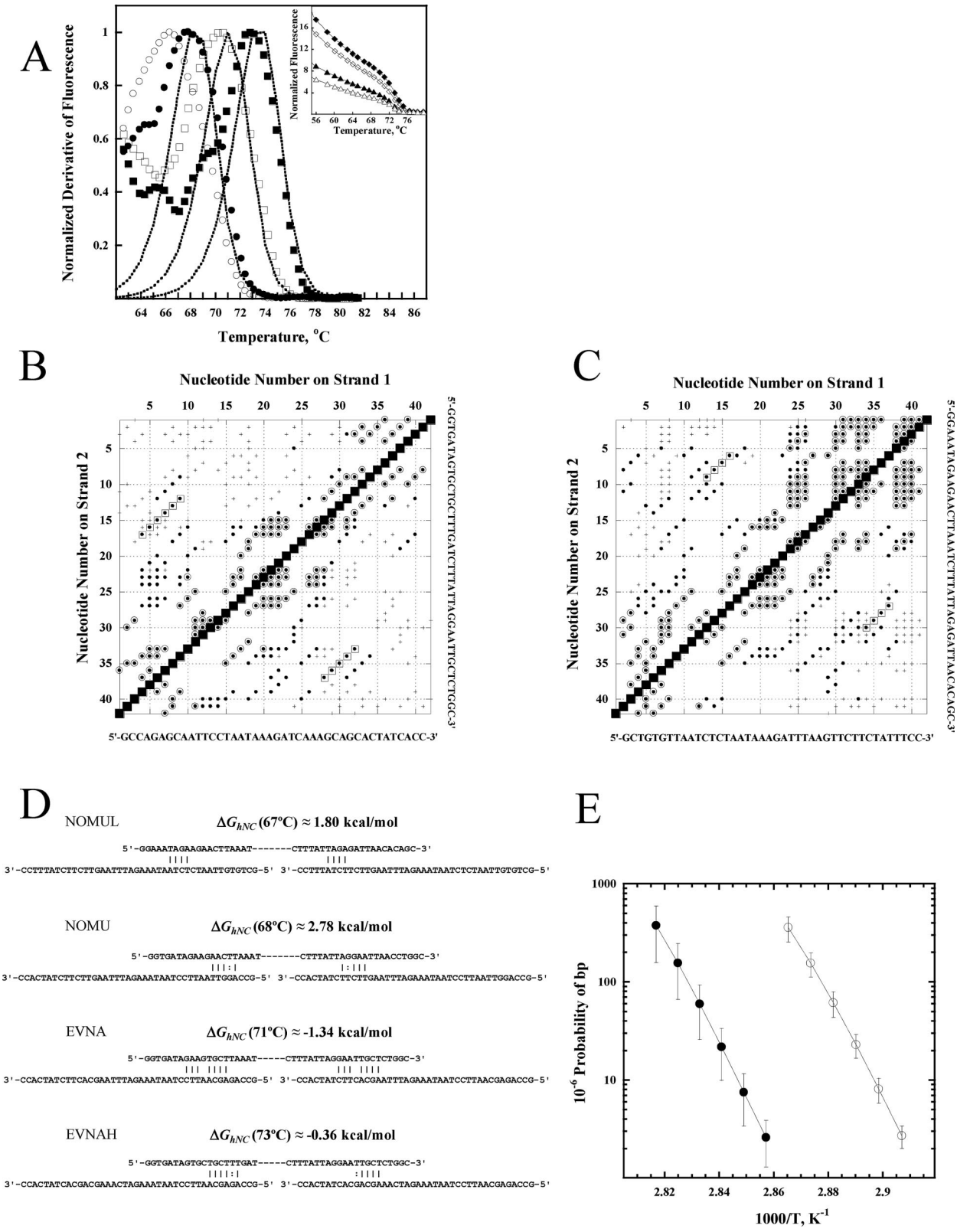

Figure 5. UNAFold predictions in the association behavior of OS single strands. (A) Experimentally observed (symbols) and predicted (dash lines) melting profiles of four OS types; open circles, NOMUL; filled in circles, NOMU; open squares, EVNA; filled in squares, EVNAH. (The predicted profiles for the OS of NOMUL and NOMU overlap.) Inset: temperature dependence of SYBR Green fluorescence with EVNAH; filled in diamonds, 160 nM; open diamonds, 80 nM; filled in triangles, 32 nM; open triangles, 16 nM. Hybridization probability dot plot of EVNAH (B) and NOMUL (C). Each symbol designates pairing between strands' nucleotides. Filled in squares designate pairs existing in OS at all tested temperatures with a probability close to 1; open circles (enclosing dots), 2nd-rank pairs at 68 °C for NOMUL and 74 °C for EVNAH; dots, pairs existing at 71 °C for NOMUL and 77 °C for EVNAH, some of which (enclosed in open squares) form bridging structures (hNC) leading to NC (Figure 1); crosses, conformations existing at 74 °C for NOMUL and at 80 °C for EVNAH. (D) Suggested structures of hNC of OS types with an approximate ΔG_{hNC} of their formation from single strands (at corresponding T_m), predicted by Visual OMP6 (conventional (|) and G:T pairings). (E) Temperature dependence of average base pair probability, with the corresponding standard deviation shown as error bars, in hNC of EVNAH (filled in circles) and NOMUL (open circles).

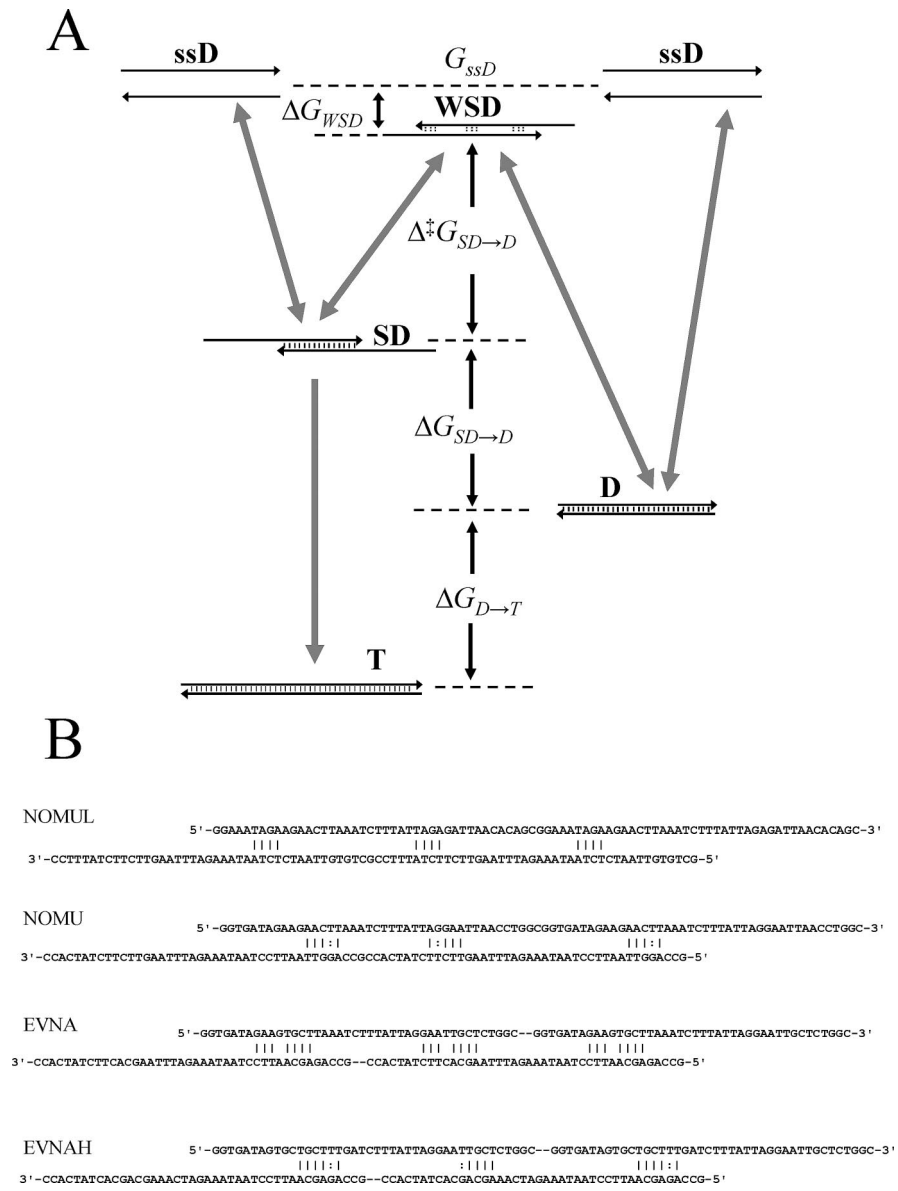

Figure 6. (A) Schematic free-energy diagram of the various conformations that participate in the suggested MPR propagation process. Dashed lines denote energy levels. G_{ssD} and $\Delta G_{D\rightarrow T}$ are, respectively, the free Gibbs energy of single-stranded D and that of the difference between T and D. (B) WSD conformations (tandem staggered OS) of the 4 D types (related to Figure 5D). (Conventional (|) and G:T pairings).

The MPR propagation was split in two processes because the annealing probability of the denatured strands of D into SD (Figure 1) is significantly lower than that into the fully complementary ("blunt") form D; having half the number of Watson−Crick bonds, the former is obviously less stable thermodynamically than the latter (the standard $\Delta G_{SD\rightarrow D}$ of the transition from SD to D is negative) (Figure 6A). Therefore, OS convert to D before the latter propagate to T and hence to a higher number of repeats. The increase of the relative prevalence of SD with temperature (justified by van't Hoff equation; see below) leads to merging of the two parallel processes (amplification and propagation) into one, transforming the MPR mode from biphasic to monophasic (gray to black arrow in Figure 2A).

NOMU is the only OS for which the MPR kinetics did not show biphasic behavior (Figure 2A), most likely because the existence of its SD conformation at all tested temperatures is sufficiently long for the overhangs to be filled in by the polymerase. Diminishing OS in MPR products with NOMU after 65 cycles by formation of higher repeat hybrid species in rapid cooling[13] (Figure 3A) substantiated this explanation. It is further verified by faster propagation to T with NOMU than with the other 3 OS types (Figure 3B) at the same time (40 cycles) and temperature (correlated with T_m). The corresponding (∼two-fold) increase in fraction of hybrid DNA (reflecting an increase in D) is demonstrated by the rapid cooling procedure[13] with all OS types (Figure 3B).

Values of $\Delta^{\ddagger}G_{ampl}$ derived from the Arrhenius plots for NOMUL and EVNAH (Figure 4A) are highly negative (around −62 kcal mole^{-1}), implying that the amplification (Figure 1) is a complex process involving a fast exothermic stage, the equilibrium constant of which decreases with temperature (Appendix). The extent of annealing of OS strands with the 3′ half of the corresponding strands of D (thus forming the hybrids H), dictated by ΔG_{OS} (Table 1), is therefore the fast-equilibrium stage that determines E. In other chemical processes as well, an exothermic fast-equilibrium stage leads to negative $\Delta^{\ddagger}G$ for the overall process.[14]

Thermodynamic Aspects of the MPR. According to the model proposed here (Figure 1), single-stranded, denatured D

(ssD) cannot readily return to D (right in Figure 6A) if it is entrapped in its SD conformation (left), despite the lower stability of the latter ($\Delta G_{SD\rightarrow D} < 0$) due to the energetic barrier ($\Delta^{\ddagger}G_{SD\rightarrow D}$) between them. The magnitude of this barrier is determined by the stability (ΔG_{WSD}) of the second-rank (intermediate), weak conformation (WSD) of D (Figure 6B). The more stable it is, the more easily SD switches to D due to smaller $\Delta^{\ddagger}G_{SD\rightarrow D}$, preventing the propagation process, thus displaying the biphasic mode of expansion (Figure 2A). Among the OS types used here, the bridging structure of NOMU is indeed the least stable (highest ΔG_{hNC}; Figure 5D), which would reflect the stability of its WSD (Figure 6B) because the latter is just a staggered tandem OS.

Approximating the first burst of the fluorescence in MPR kinetics (Figure 2A) by eq 1 allows more precise determinations of E and R. The high variability in the Arrhenius plots (Figure 4A) seems to result from limited accuracy of the temperature maintenance by the heat block of the RT-PCR apparatus for the duration of each cycle (repeatedly launched by rapid cooling from 95 °C to the desired temperature). The actual temperature that acts on each hexaplicate may therefore differ from the registered one. The temperature-dependent amplification rate A (Figure 4A) was used alternatively as a more stable indicator because it reflects the average temperature during the cycle. At all rates (indicating the operative temperature above the respective T_m), the calculated ratios [ID]/[OS] (R^{-1} of eq 1) for NOMUL are lower than those for EVNAH (Figure 4B). The relative propensity for ID formation from NOMUL is thus lower than that for EVNAH, consistent with lower stability of the putative bridging structure involved in NC formation of NOMUL than that for EVNAH (Figure 5D).

The relative probability of second-rank structures formed by OS and D, supposedly involved in MPR initiation (bridging structures hNC; Figures 1 and 5D) and in propagation (staggered structures SD; Figure 6A) increases with temperature (Figures 4B and 2A, respectively). This trend is predicted by UNAFold software (Figures 3C and 5E). The van't Hoff equation that formulates this tendency is

$$\frac{\mathrm{d}\ \ln\ K_{1st\rightarrow 2nd}}{\mathrm{d}(1/T)} = -\frac{\Delta H_{1st\rightarrow 2nd}}{R}$$

where $K_{1st\rightarrow 2nd}$ and $\Delta H_{1st\rightarrow 2nd}$ are, respectively, the equilibrium constant and the standard enthalpy for the transition between more stable first-rank (OS and D) and less stable second-rank (hNC and SD) structures. $\Delta H_{1st\rightarrow 2nd} > 0$ because the stability of second-rank structures is lower. Therefore, as the temperature increases ($1/T$ decreases), ln $K_{1st\rightarrow 2nd}$ and hence $K_{1st\rightarrow 2nd}$ must increase, reflecting a rise in the probability of the second-rank conformations. However, the increase with temperature of alternative OS pairings (crosses in Figure 5B and C) lowers the efficiency of the MPR initiation from the hNC structure (dots enclosed in open squares in Figure 5B and C). This decrease in efficiency of the MPR initiation is probably reflected in the experimentally observed bend (Figure 4B) at low amplification rates corresponding to relatively high temperatures (Figure 4A).

Concordance between the experimentally observed behavior of OS and D and that predicted by UNAFold lends additional support to the conclusions arrived at here on the one hand and to the predictive capability of the program on the other. The overestimated observed fluorescence in the melting profiles (ascending parts in Figure 5A) can be explained by the temperature dependence of the equilibrium constant of double-stranded DNA association with intercalating agents (first phase in the lines of the inset in Figure 5A). The steeper, second phase reflects strand separation (melting itself), whereas the first (between 56 and 72 °C for EVNAH) results from release of the intercalated dye from OS due to the negative enthalpy of this latter process.[15]

Conclusions

Thermodynamic substantiation of the model[12] that explains the MPR is based on different propensities of various HDs to expand into multiple repeating units, as previously obtained.[5] These tendencies are justified experimentally in terms of different stabilities of NCs engaged in MPR initiation. In addition, a new stage of the MPR (named amplification) emerged from observing biphasic kinetics with some HDs. UNAFold-aided simulations agreed satisfactorily with experimental results, thus further supporting the established model.

MPR with nonrepetitive HD presents an optional chemical evolutionary system in which the thermodynamic advantage of specific, very weak interactions that exist in second-rank DNA structures is selected for biased proliferation of a certain reaction product.[3] The learned approach to optimize MPR is necessary in protein engineering. The importance of studying this phenomenon lies far beyond applied interest; it may reflect primordial molecular evolution of primitive DNA sequences into complex genomes.

Acknowledgment. This investigation was partially supported by Eshkol Fellowship, Ministry of Science, Jerusalem, Israel, (to M.I.) and the United States−Israel Binational Science Foundation (BSF), Jerusalem, Israel (Grants # 2001-042 and 2007037 to A.Z.). Thanks are due to Michael Zuker and Idan Gabdank for assistance in UNAFold simulations, to Eitan Ben-Dov for help in performing RT-PCR, and to DNA Software Inc. for providing a free 7 day trial license to Visual OMP, version 6.3.

Appendix

The amplification (multiplying ID using OS; Figure 1) can be formulated by the chemical equation

$$\mathrm{OS} + \mathrm{D} \overset{\mathrm{I}}{\leftrightarrow} 2\mathrm{H} \overset{\mathrm{II}}{\rightarrow} 2\mathrm{D}$$

where I and II denote the first (fast equilibrium) and second (rate-limiting) steps of the process. The rate of amplification (II) can be expressed as $\mathrm{d[D]}/\mathrm{d}t = k[\mathrm{H}]$, where k is the rate constant of the rate-limiting step. At temperatures higher than the T_m of OS (and obviously of H) and lower than that of D, step I involves melting of OS, fraying the ends of D, and hybridization of the single strands of the former with the latter. Assuming that this step occurs near its multistate equilibrium, with $K_H = [\mathrm{H}]/([\mathrm{OS}][\mathrm{D}])$, the overall process is expressed by $\mathrm{d[D]}/\mathrm{d}t = kK_H[\mathrm{OS}][\mathrm{D}]$. The k rises with temperature, but K_H decreases due to the dissociation of H into D and single-stranded OS. In this reaction, k rises less than the drop in K_H, so that the overall value kK_H decreases with temperature.

If the amount of OS that turns into D is x (the progress variable), $[\mathrm{D}] = [\mathrm{D}]_0 + x$, $[\mathrm{OS}] = [\mathrm{OS}]_0 - x$, and the rate of change of either species is

$$\frac{\mathrm{d}x}{\mathrm{d}t} = kK_H([\mathrm{D}]_0 + x)([\mathrm{OS}]_0 - x)$$

Integration of this equation, using

$$\frac{1}{([D]_0 + x)([OS]_0 - x)} = \frac{1}{[D]_0 + [OS]_0} \times \left(\frac{1}{[D]_0 + x} + \frac{1}{[OS]_0 - x}\right)$$

and $t = N\varepsilon$ (where N is the number of cycles and ε is the cycle period), yields

$$\frac{1}{[D]_0 + [OS]_0} \ln\left(\frac{[OS]_0([D]_0 + x)}{[D]_0([OS]_0 - x)}\right) = kK_H N\varepsilon$$

This expression can be rearranged into

$$x = \frac{[OS]_0(e^{AN} - 1)}{[OS]_0/[D]_0 + e^{AN}}$$

where $A = kK_H\varepsilon([OS]_0 + [D]_0)$.

The measured total fluorescence is $Flu_{Tot} = \alpha([OS] + \gamma[D])$ or

$$Flu_{Tot} = \alpha\left([OS]_0 - \frac{[OS]_0(e^{AN} - 1)}{[OS]_0/[D]_0 + e^{AN}}\right) + \alpha\gamma\left([D]_0 + \frac{[OS]_0(e^{AN} - 1)}{[OS]_0/[D]_0 + e^{AN}}\right)$$

where α is the extinction coefficients of OS and γ is the ratio between the extinction coefficients of OS and D. After rearrangement

$$Flu_{Tot} = \alpha[OS]_0 + \alpha\gamma[D]_0 + \alpha(\gamma - 1)\frac{[OS]_0(e^{AN} - 1)}{[OS]_0/[D]_0 + e^{AN}}$$

$[D]_0$ ($[ID]$) is negligible relative to $[OS]_0$; therefore, this expression can be approximated to

$$Flu_{Tot} = \alpha[OS]_0\left(1 + (\gamma - 1)\frac{(e^{AN} - 1)}{[OS]_0/[D]_0 + e^{AN}}\right)$$

$$= Flu_{Bgr}\left(1 + (\gamma - 1)\frac{(e^{AN} - 1)}{R + e^{AN}}\right)$$

where $Flu_{Bgr} = \alpha[OS]_0$ and $R = [OS]_0/[D]_0$.

References and Notes

(1) Shiba, K.; Takahashi, Y.; Noda, T. *Proc. Natl. Acad. Sci. U.S.A.* **1997**, *94*, 3805.
(2) Shiba, K.; Shirai, T.; Honma, T.; Noda, T. *Protein Eng.* **2003**, *16*, 57.
(3) Saito, H.; Minamisawa, T.; Shiba, K. *Nucleic Acids Res.* **2007**, *35*, e38.
(4) Shiba, K.; Minamisawa, T. *Biomacromolecules* **2007**, *8*, 2659.
(5) Itsko, M.; Zaritsky, A. *FEBS Lett.* **2007**, *581*, 1775.
(6) Margolis, R. L.; Ross, C. A. *Trends Mol. Med.* **2001**, *7*, 479.
(7) Liquori, C. L.; Ricker, K.; Moseley, M. L.; Jacobsen, J. F.; Kress, W.; Naylor, S. L.; Day, J. W.; Ranum, L. P. *Science* **2001**, *293*, 864.
(8) Matsuura, T.; Yamagata, T.; Burgess, D. L.; Rasmussen, A.; Grewal, R. P.; Watase, K.; Khajavi, M.; McCall, A. E.; Davis, C. F.; Zu, L.; Achari, M.; Pulst, S. M.; Alonso, E.; Noebels, J. L.; Nelson, D. L.; Zoghbi, H. Y.; Ashizawa, T. *Nat. Genet.* **2000**, *26*, 191.
(9) Heidenfelder, B. L.; Topal, M. D. *Nucleic Acids Res.* **2003**, *31*, 7159.
(10) Harvey, S. C. *Biochemistry* **1997**, *36*, 3047.
(11) Tuntiwechapikul, W.; Salazar, M. *Biochemistry* **2002**, *41*, 854.
(12) Itsko, M.; Zaritsky, A.; Rabinovitch, A.; Ben-Dov, E. *Biochem. Biophys. Res. Commun.* **2008**, *368*, 606.
(13) Hershey, A. D.; Burgi, E. *Proc. Natl. Acad. Sci. U.S.A.* **1965**, *53*, 325.
(14) Atkins, P. W. *Physical Chemistry*, 5th ed.; Oxford University Press: New York, 1994; p 887.
(15) Biver, T.; De Biasi, A.; Secco, F.; Venturini, M.; Yarmoluk, S. *Biophys. J.* **2005**, *89*, 374.

JP8045142